Check for updates

Magnetic Resonance Imaging Evaluation of Perivascular Space Abnormalities in Neuromyelitis Optica

Laura Cacciaguerra, MD,[1,2,3] Antonio Carotenuto, MD,[1] Elisabetta Pagani, MSc,[1] Damiano Mistri, MSc,[1] Marta Radaelli, MD, PhD,[2] Vittorio Martinelli, MD,[2] Massimo Filippi, MD,[1,2,4,5,3] and Maria A. Rocca, MD[1,2,3]

Objective: Astrocytes outline the perivascular space (PVS) and regulate fluid exchange through the aquaporin-4 water channel. As neuromyelitis optica is an autoimmune astrocytopathy targeting aquaporin-4, we hypothesized that it could be associatied with PVS abnormalities.

Methods: A total of 34 patients, and 46 age- and sex-matched healthy controls from two independent cohorts (exploratory and validation dataset) underwent a standardized 3.0-T magnetic resonance imaging protocol including conventional and diffusion tensor imaging. Susceptibility-weighted imaging was also acquired in the exploratory dataset. We evaluated macroscopic and microstructural abnormalities of PVS in terms of enlargement and water diffusivity (DTI-ALPS index). In the exploration dataset, a susceptibility-weighted sequence was used to draw the regions of interest for the DTI-ALPS index calculation in areas having veins perpendicular to lateral ventricles. Between-group comparisons, correlations, and regression models were run to assess associations between PVS abnormalities, and clinical and magnetic resonance imaging variables.

Results: Patients had a higher frequency of severe PVS enlargement in the centrum semiovale (29.4% vs 8.7%), which correlated with brain atrophy, deep grey matter atrophy, and poorer cognitive performance (r-values range: −0.44, −0.36; p values: 0.01–0.046).

In both datasets, patients had reduced DTI-ALPS index compared with controls (p values 0.004–0.038). Lower DTI-ALPS index, deep gray matter volume, and cortical volume could discriminate between patients and controls ($R^2 = 0.62$), whereas lower DTI-ALPS index, higher number of myelitis, and higher T2-lesion volume were associated with worse disability ($R^2 = 0.55$).

Interpretation: Patients with neuromyelitis optica spectrum disorder are characterized by abnormal enlargement and impaired water diffusion along the PVS, whose clinical implications suggest a direct correlation with disease pathogenesis and severity.

ANN NEUROL 2022;92:173–183

Introduction

In the central nervous system, astrocytes are at the interface between the vascular tree and the brain parenchyma. Their endfeet envelope the abluminal surface of blood vessels as part of the blood–brain barrier, and delimit the perivascular space.[1]

Neuromyelitis optica spectrum disorder (NMOSD) is an autoimmune astrocytopathy caused by autoantibodies targeting the aquaporin-4 (AQP4) water channel,[2,3] a protein that guarantees brain water homeostasis through fluid influx and efflux.[4]

View this article online at wileyonlinelibrary.com. DOI: 10.1002/ana.26419

Received Dec 22, 2021, and in revised form May 19, 2022. Accepted for publication May 19, 2022.

Address correspondence to Prof Rocca, Neuroimaging Research Unit, Division of Neuroscience, IRCCS San Raffaele Scientific Institute, Milan, Italy. E-mail: rocca.mara@hsr.it

From the [1]Neuroimaging Research Unit, Division of Neuroscience, IRCCS San Raffaele Scientific Institute, Milan, Italy; [2]Neurology Unit, IRCCS San Raffaele Scientific Institute, Milan, Italy; [3]Vita-Salute San Raffaele University, Milan, Italy; [4]Neurorehabilitation Unit, IRCCS San Raffaele Scientific Institute, Milan, Italy; and [5]Neurophysiology Service, IRCCS San Raffaele Scientific Institute, Milan, Italy

© 2022 The Authors. *Annals of Neurology* published by Wiley Periodicals LLC on behalf of American Neurological Association.
This is an open access article under the terms of the Creative Commons Attribution-NonCommercial-NoDerivs License, which permits use and distribution in any medium, provided the original work is properly cited, the use is non-commercial and no modifications or adaptations are made.

As AQP4 is highly expressed on the astrocytes' membrane abutting the perivascular space, this site is likely injured in NMOSD, as also suggested by pathology studies showing a vasculocentric pattern of antibody deposition and complement activation.[5]

Enlarged perivascular spaces, also referred as Virchow–Robin spaces, are visualized by using conventional T2- or T1-weighted magnetic resonance imaging (MRI) sequences, as fluid-filled structures paralleling perforating vessels in the basal ganglia and centrum semiovale.[6]

As perivascular spaces have a three-dimensional tubular geometry, it was hypothesized that the diffusion of water molecules in this space is anisotropic (ie, preferentially parallels the main vessel direction).[7] This was confirmed with 7.0-T MRI using multishell diffusion imaging, an advanced technique able to separate the anisotropic movement of water molecules within white matter tracts, from the less constrained diffusion in the non-parenchymal compartment, including the perivascular space.[7]

However, the diffusion along perivascular spaces can also be measured at lower field strengths exploiting diffusion tensor imaging (DTI), in association with susceptibility-weighted imaging for vessel visualization. Accordingly, the diffusion along perivascular spaces (DTI-ALPS index) can be calculated as the ratio of (i) water diffusivity parallel to vessels, and (ii) the set of diffusivities perpendicular to white matter tracts.[8] Therefore, this technique can be considered as a stratagem to solve the problem in a known and simpler anatomical configuration when multishell diffusion-weighted data are not available.

Both perivascular space enlargement and decreased water diffusion along the perivascular spaces have been found in a number of neurological conditions, including cerebrovascular diseases,[6,9] neurodegenerative,[8,10] and inflammatory disorders.[6,11]

Although the mechanism is not fully understood, these observations have raised the hypothesis that perivascular space abnormalities could be a common feature of several neurological diseases.[9]

NMOSD autoimmunity involves an antigen highly expressed in the perivascular space (ie, AQP4), and leads to damage of its anatomical borders (ie, astrocytes).[3] Therefore, we explored macroscopic and microstructural perivascular space abnormalities in NMOSD by quantifying perivascular space enlargement, and by measuring the DTI-ALPS index, respectively. Then, we assessed associations between these measures, clinical, and MRI outcomes.

Methods

Ethics Committee Approval

Ethical approval was received from the local ethical standards committee, and written informed consent was obtained from all participants at the time of data acquisition. Specifically, patients agreed to undergo a research MRI scan, and a neurological and neuropsychological examination without any clinical purpose.

Participants

We computed the DTI-ALPS index in two independent cohorts (exploratory dataset and validation dataset) of age- and sex-matched right-handed NMOSD patients and healthy controls (HCs) acquired using two different MRI scanners and standardized acquisition protocols.

The exploratory dataset included 14 NMOSD patients and 16 HCs acquired between February 2007 and December 2011; whereas the validation dataset included 20 NMOSD patients and 30 HCs acquired between April 2019 and June 2021.

NMOSD diagnosis was achieved according to the 2015 International Panel Consensus Diagnostic criteria.[2] For all participants, exclusion criteria were any contraindication to MRI, history of head trauma, psychiatric comorbidities, and alcohol or drug abuse. Patients were evaluated during the remission phase of the disease (ie, at least 4 weeks apart from clinical relapse and intravenous steroids administration).

Clinical Evaluation

Within 48 hours from the MRI acquisition, patients underwent a clinical examination with rating of the Expanded Disability Status Scale (EDSS)[12] and collection of disease history (ie, disease duration, and number and type of previous relapses). A total of 28 of 34 patients (82.4%) also agreed to undergo a neuropsychological assessment including the Brief Repeatable Battery of Neuropsychological Tests. As former studies showed that information processing speed/attention domain is the most frequently impaired in NMOSD patients,[13,14] we analyzed the performance at the symbol digit modalities test and Paced Auditory Serial Addition Test 3″ as cognitive screening. Results were converted in z-scores based on Italian normative data after subtracting the effects of relevant variables (ie, education, sex) as described elsewhere.[15] The presence of at least one abnormal test (ie, corrected score <1.5 standard deviations compared with the reference population) defined the presence of impairment in the domain.[16]

MRI Acquisition

All participants underwent a single brain MRI session using two 3.0-T scanners (Ingenia CX and Intera Philips Medical Systems; Amsterdam, the Netherlands). To minimize possible intersubject variability secondary to sleeping status, all participants were acquired between 1 p.m. and 8 p.m., according to the following protocols:

1.Exploratory-dataset: (i) sagittal 3D fluid-attenuated inversion recovery, field of view (FOV) 256 × 256 mm, pixel size 1 × 1 mm, 192 slices, 1-mm thick, matrix 256 × 256, repetition time (TR) 4,800 ms, echo time 270 ms, inversion time 1,650 ms, and echo train length 167; (ii) sagittal 3D T2-weighted sequence, FOV 256 × 256 mm^2, pixel size 1 × 1 mm, 192 slices, 1-mm thick, matrix 256 × 256, TR 2,500 ms, TE 330 ms, and echo train length 117; (iii) sagittal 3D T1-weighted magnetization-prepared rapid gradient echo, FOV 256 × 256, pixel size 1 × 1 mm, 204 slices, 1-mm thick, matrix 256 × 256, TR 7 ms, TE 3.2 ms, inversion time 1,000 ms, and flip angle 8°; (iv) axial pulsed-gradient spin echo single shot diffusion-weighted echo planar imaging; three shells at b-value 700/1,000/2,855 seconds/mm^2 along 6/30/60 non-collinear directions and 10 b = 0 volumes were acquired, FOV 240 × 233 mm, pixel size 2.14 × 2.69 mm, 56 slices, 2.3-mm thick, matrix 112 × 85, TR 5,900 ms, TE 78 ms, and three additional b = 0 volumes with reversed polarity of gradients for distortion correction; (v) 3D susceptibility weighted image (SWI), FOV 230 × 230, pixel size 0.60 × 0.60 mm, 135 slices, 2-mm thick, matrix 384 × 382, TR 39 ms, TE 5.5:6:35.5 ms, and flip angle 17; both magnitude and phase images for each echo were saved.

2.Validation-dataset: (i) axial dual-echo turbo spin-echo, FOV 240 × 240 mm^2, 44 slices, 3-mm thick, matrix 256 × 256, pixel size 0.94 × 0.94 mm, TR 2599 ms, TE 16–80 ms, echo train length 6, and flip angle 90°; (ii) axial 3D T1-weighted fast gradient-echo (fast field echo), FOV 230 × 230 mm, 220 slices, 0.8-mm thick, matrix 256 × 256, pixel size 0.89 × 0.89 mm, TR 25 ms, TE 4.6 ms, and flip angle 30°; (iii) axial pulsed-gradient spin echo diffusion-weighted echo-planar imaging, single shell at b-value 900 s/mm^2 along 35 non-collinear directions, FOV 240 × 231 mm, pixel size 2.14 × 2.62 mm, 56 slices, 2.3 mm-thick, matrix 112 × 88, SENSE 2, TR 8692 ms, and TE 58 ms.

MRI Analysis

Conventional MRI analysis. In the exploratory dataset, focal white matter (WM) lesions were segmented using a fully automated approach based on two 3D patch-wise convolutional neural networks with 3D fluid-attenuated inversion recovery and 3D T1-weighed MR images as inputs.[17] In the validation dataset, a local thresholding segmentation technique was adopted to segment T2-hyperintense lesions on T2-weighted sequences (Jim 8.0 Xinapse System Ltd, Essex, UK). Corresponding lesion masks and volumes were then computed.

After lesion refilling,[18] we measured head-size normalized volumes of the brain using SIENAx[19] and deep gray matter (NDGM) with FMRIB's Integrated Registration and Segmentation Tool (FIRST) software.[20] NDGM volume was obtained by summing up volumes of the bilateral thalamus, caudate, putamen, pallidum, amygdala, and accumbens. We also obtained cortical volumes (normalized for head size) using Freesurfer 6.0. (https://surfer.nmr.mgh.harvard.edu).

Evaluation of enlarged perivascular spaces. According to the Potter's score, the presence of perivascular space enlargement was assessed visually on axial T2-weighted images in the basal ganglia and WM of the centrum semiovale using a 0 to 4 semiquantitative scoring system. Briefly, a score equal to 0 corresponds to the absence of enlarged perivascular spaces, 1 to 1–10, 2 to 11–30, 3 to 21–40, and 4 to >40 enlarged perivascular spaces per region.[21]

Pre-processing of diffusion-weighted imaging. Pre-processing of diffusion-weighted images included correction for off-resonance (exploratory dataset) and eddy current-induced distortions and movements using the Eddy tool in the FSL library.[22] The diffusion tensor was estimated by linear regression on diffusion-weighted imaging data at b = 700/1,000 s/mm^2 (exploratory-dataset) or b = 900 s/mm^2 (validation-dataset). Then, maps of fractional anisotropy (FA) and mean diffusivity (MD) were derived from the diffusion tensor.[23]

Processing of SWI. The multi-echo SWIs were used as inputs to obtain maps of local B0 field changes (where venous vessels are visible) using the software available at https://github.com/sunhongfu/QSM. First, phase images were unwrapped using the best path method to eliminate any discontinuity due to the limited range of phase values.[24] Then, the unwrapped phase images were fitted to the TE using a magnitude-weighted least-square regression. Small veins were made visible by removing the global spatial changes of the main magnetic field using regularization enabled sophisticated harmonic artifact reduction for phase data.[25]

Quantification of DTI-ALPS index. As SWI sequence was available in the exploratory dataset only, we overcame the lack of SWI images in the validation dataset by setting an automated system of regions of interest (ROIs) positioning on diffusion-weighted images based on the ROIs probability maps identified in this dataset, as summarized in Figure, panel A.

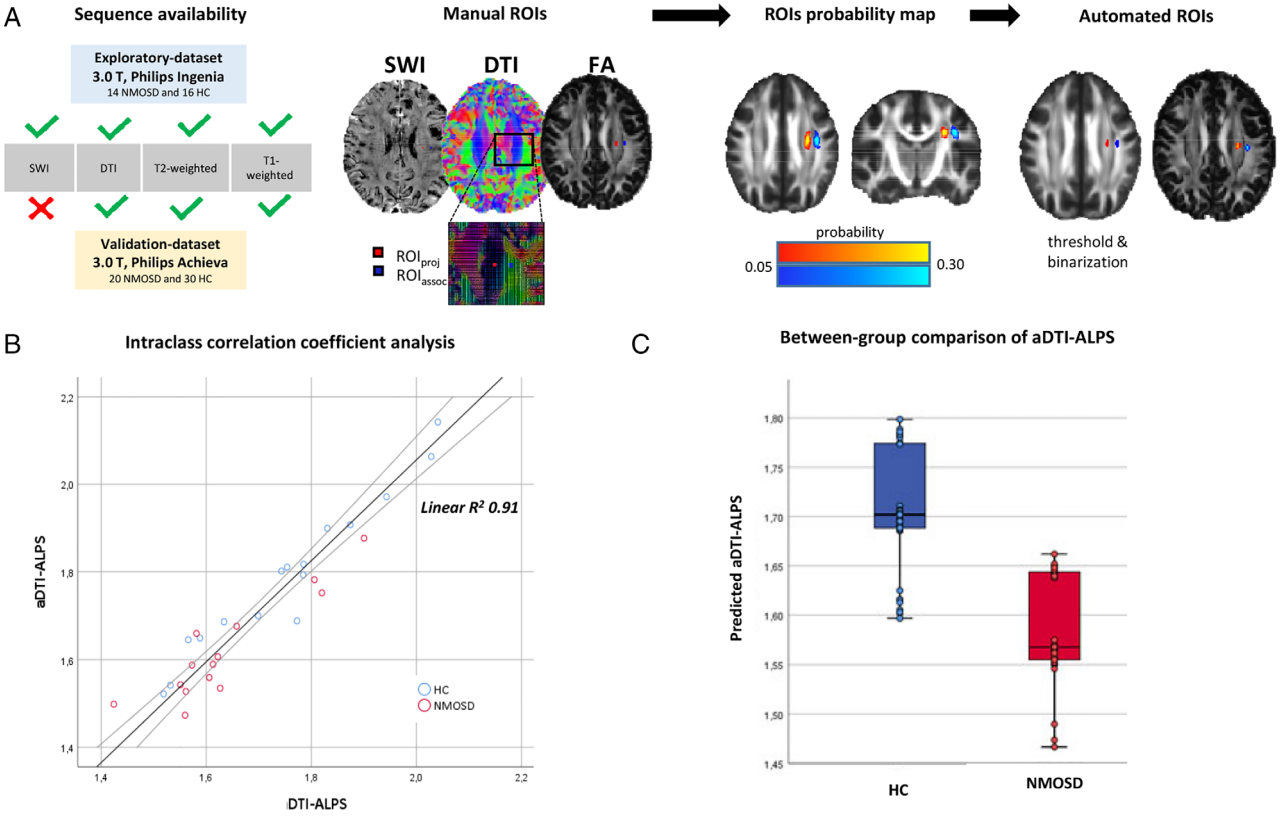

FIGURE: DTI-ALPS index measurement in the two datasets. (A) Susceptibility-weighted images (SWI) were available in the exploratory dataset only. In this dataset, after choosing three contiguous slices with veins perpendicular to ventricles on SWI, we manually placed one region of interest (ROI) on projection fibers (ROI_{proj} in red) and a second ROI on associative fibers (ROI_{assoc}, in blue) on color-coded principal diffusion direction map. Then, we obtained ROI probability maps in a standard space, which were 0.25 thresholded and binarized into two automated ROIs (aROI). Finally, $aROI_{proj}$ and $aROI_{assoc}$ were moved back to the single-subject diffusion imaging space. (B) An absolute agreement intraclass correlation analysis was run to validate the use of aROIs on the validation dataset. The graphic shows the scatterplot of the linear correlation between manual and automated DTI-ALPS index. (C) Scatterbox of age-, sex-, and scanner-adjusted predicted values of aDTI-ALPS index in healthy controls (HC; blue box) and neuromyelitis optica spectrum disorder patients (NMOSD; red box). Abbreviations: DTI = diffusion-tensor imaging; (a) DTI-ALPS = (automated) diffusion along perivascular space; FA = fractional anisotropy; HC = healthy controls; NMOSD = neuromyelitis optica spectrum disorders; ROI_{assoc} = regions of interest in associative fibers; ROI_{proj} = regions of interest in projective fibers; SWI = susceptibility-weighted images.

Exploratory Dataset

1. *Manual positioning of ROIs (single-subject space)*: for each subject, we performed a rigid registration onto the SWI space of the FA map, 3D fluid-attenuated inversion recovery images, T2 lesion masks, and the principal diffusion direction field (first eigenvector) using the magnitude of the first echo of the SWI sequence as the reference image through FMRIB's Linear Image Registration Tool.[26] Using SWI-derived venous images, we identified three contiguous axial slices having veins running perpendicular to lateral ventricles. Then, using the color-coded principal diffusion direction map, we manually drew two 3 × 3 × 3-mm cubic ROIs over these slices in the left (ie, dominant) hemisphere.[11,27] The first ROI (ROI_{proj}) was positioned in projection fibers, the second ROI (ROI_{assoc}) was placed in the area of associative fibers.[11] We included only right-handed participants to ensure an adequate thickness of the left hemisphere's associative fibers, to minimize the possibility of losing the condition of perpendicularity between the fiber axis and the perivenous space, as previously described.[8] A T2 lesion mask was used to avoid placing ROIs over visibly damaged tissue.

ROIs were then moved to the native diffusion imaging space by applying the inverse diffusion-to-SWI linear transformation. Diffusivity values along the *x*-, *y*-, and *z*-axes were then extracted for each ROI, and the DTI-ALPS index was calculated as the ratio of diffusivities perpendicular to fiber bundles and parallel to veins (Dx_{proj} and Dx_{assoc}) over diffusivities perpendicular to fiber bundles and veins (Dy_{proj} and Dz_{assoc}).[8] This was obtained by exploiting the frame of reference built with diffusion tensor eigenvectors and the associated eigenvalues.[11] We also verified that secondary and tertiary

eigenvectors were not affected by sorting bias.[28] DTI-ALPS index was calculated using the following formula:

$$DTI-ALPS\ index = \frac{mean(Dx\ proj, Dx\ assoc)}{mean(Dy\ proj, Dz\ assoc)}$$

For descriptive purposes, we also measured the mean FA and MD within the two ROIs.

2. *Automated positioning of ROIs (standard space)*: from the single-subject diffusion imaging space, all ROIs were then registered in a standard space by applying the nonlinear FA to standard space transformation obtained from the second step of the Tract-Based Spatial Statistics.[29] Mean ROI probability maps were produced separately for each ROI (ROI_{proj} and ROI_{assoc}). A threshold of 0.25 was applied to retain only voxels occupied by ROI_{proj} and ROI_{assoc} in at least 25% of participants, and the map obtained was binarized into two automated ROIs ($aROI_{proj}$ and $aROI_{assoc}$). Finally, $aROI_{proj}$ and $aROI_{assoc}$ were registered to the subject diffusion imaging space by applying the inverse FA to standard space transformation. Diffusivity values along the *x*-, *y*-, and *z*-axes were then extracted for each aROI, as previously described, to calculate the automated DTI-ALPS (aDTI-ALPS) index with the same formula. A linear correlation and the absolute agreement of the intraclass correlation coefficient (ICC) were used to assess the agreement between the DTI-ALPS index and the aDTI-ALPS index.

Validation Dataset. Using Tract-Based Spatial Statistics, FA images of subjects were registered onto the customized FA atlas previously obtained with Tract-Based Spatial Statistics for the exploratory-dataset, where diffusivity values within the $aROI_{proj}$ and $aROI_{assoc}$ were extracted. Then, $aROI_{proj}$ and $aROI_{assoc}$ were transformed back to single-subject space. Before calculation of the aDTI-ALPS index, we visually checked that aROIs did not overlap with WM lesions.

Statistical Analysis

After exploring the normal distribution of continuous variables with the Kolmogorov–Smirnov test, demographic, clinical, and conventional MRI variables were compared between groups using two-sample *t* test or Mann–Whitney *U* test as approapriate. T2 WM lesion volumes were log-transformed to normalize their distribution. We grouped perivascular space scores in three categories: mild or no enlargement (scores 0–1), moderate enlargement (score 2), and frequent or severe enlargement (scores 3–4). The distribution of categorical variables was assessed with Pearson's χ^2 or Fisher's exact test.

Between-group comparisons of aDTI-ALPS index in the exploratory and validation dataset were performed separately with the nonparametric Mann–Whitney *U* test. Age-, sex-, and scanner-adjusted general linear models were used to explore between-group differences of the aDTI-ALPS index using pooled data from the two datasets.

Correlations between the aDTI-ALPS index, perivascular space scores, demographic, clinical, neuropsychological, and MRI variables were assessed in the pooled cohort of NMOSD patients, using age-, sex-, and scanner-adjustement when appropriate.

Finally, stepwise age-, sex-, and scanner-adjusted multiple regression models were run to assess predictors of NMOSD diagnosis or impairment in information processing speed/attention domain (binary logistic regression) and clinical disability (linear logistic regression). In the stepwise variable selection, a p value = 0.10 was retained for entry in the multivariate model. Dependent variables were: aDTI-ALPS index, perivascular space scores in the basal ganglia and centrum semiovale, logT2 lesion volumes, normalized volumes of the brain, NDGM, and the mean normalized cortical volume. All statistical analyses were performed with SPSS software (version 26.0; IBM, Armonk, NY, USA). A p value <0.05 was considered statistically significant.

Results

Demographic, Clinical, and Conventional MRI Measures

Tables 1 and 2 summarize the main demographic, clinical, and MRI features of study participants.

NMOSD patients of the two datasets did not differ in terms of disease duration, EDSS, number of previous optic neuritis, and number of previous myelitis (p values range 0.19–0.69). All NMOSD patients in the exploratory dataset and 70% patients in the validation dataset were under chronic immunosuppressive treatment at the time of the MRI acquisition. This included nonbiologic immunosuppressants (ie, azathioprine, $n = 7$, micophenolate mophetil, $n = 1$, cyclophosphamid, $n = 1$), oral steroids ($n = 3$, always administered in add-on), and monoclonal antibodies (rituximab, $n = 16$, tocilizumab, $n = 2$). In line with the different historical moment, the frequency of monoclonal antibody administration was higher in the exploratory dataset.

Autoimmune connective tissue disorders were detected in two patients (6%), and included one case of Sjögren's syndrome and one undifferentiated connectivitis; antiphospholipid antibodies were positive in two patients (6%).

TABLE 1. Demographic and Clinical Variables in the Two Datasets

	Exploratory-dataset			Validation-dataset			NMOSD[c]	HC[c]
	NMOSD ($n = 14$)	HC ($n = 16$)	p	NMOSD ($n = 20$)	HC (n = 30)	p	p	p
Demographic and clinical features								
Mean age (SD) [years][a]	48.5 (10.2)	48.4 (10.9)	0.98	46.9 (14.2)	44.1 (13.6)	0.90	0.73	0.29
F/M	14/0	13/3	0.23	17/3	22/8	0.49	0.25	0.72
Disease duration	4.5 (1; 10)	–	–	8.2 (3;17)	–	–	0.19	–
EDSS	3.5 (1.5; 6.5)	–	–	4.0 (1.75; 6.75)	–	–	0.69	–
n myelitis	2.0 (0.75; 3.5)	–	–	2.0 (1.0; 4.5)	–	–	0.69	–
n optic neuritis	0.5 (0; 5.5)	–	–	2.0 (0.25; 4.0)	–	–	0.48	–
Autoimmune connective tissue disorders (%)	2 (14%)	–	–	0 (0%)	–	–	0.16	–
Antiphospholipids antibodies (%)	1 (7%)	–	–	1 (5%)	–	–		–
Impairment in IPS/attention (%)	2 (18%)[d]	–	–	10 (59%)[e]	–	–	0.05	–
SDMT	−0.48 (−1.0; 0.7)	–	–	−1.12 (−2.5; −0.8)	–	–	**0.049**	–
PASAT-3	−0.76 (−1.1; 0.3)	–	–	−1.42 (−2.4; 0.0)	–	–	0.11	–
Treatment (%)[b]	14 (100%)	–	–	14 (70%)	–	–	**0.03**	–
Immunosoppressants (%)	3 (21%)	–	–	6 (30%)	–	–	0.70	–
Oral steroids (%)	0 (0%)	–	–	3 (15%)	–	–	0.25	–
Monoclonal antibodies (%)[b]	11 (79%)	–	–	7 (35%)	–	–	**0.01**	

[a]Two-sample t test.
[b]Pearson χ^2.
[c]Exploratory versus validation dataset.
[d]n = 11.
[e]n = 17.
Data are presented as median (IQR). Unless otherwise specified, p values refer to nonparametric Mann–Whitney U test (quantitative variables) or Fisher's exact test (qualitative variables).
EDSS = expanded disability status scale; F/M = female/male ratio; HC = healthy controls; NMOSD = neuromyelitis optica spectrum disorders; PASAT-3 = Paced Auditory Serial Addition Test 3″ z-score; SD = standard deviation; IPS = information processing speed; SDMT = symbol digit modalities test z-score.

The between-group comparison of NMOSD patients and HCs showed significant cortical atrophy in both datasets (p values range 0.019–0.023), whereas we detected a significant deep GM atrophy only in the validation-dataset ($p = 0.003$).

Perivascular Space Scoring

The scoring of MRI-visible perivascular spaces was similar between NMOSD and HCs in the basal ganglia (p values range 0.17–0.26). In the centrum semiovale, NMOSD patients had a higher frequency of severe perivascular

TABLE 2. Between-Group Comparison of Magnetic Resonance Imaging Variables and Virchow–Robin Space Enlargement Score Distribution

		Exploratory-dataset			Validation-dataset		
		NMOSD (n = 14)	HC (n = 16)	*p*	NMOSD (n = 20)	HC (n = 30)	*p*
Conventional MRI variables (ml)							
T2 LV		7.1 (5.9–7.8)	–	–	5.9 (5.1–7.1)	–	–
NBV		1,541 (1,527–1,591)	1,565 (1,555–1,583)	0.32	1,545 (1,509–1,574)	1,578 (1,531–1,635)	0.08
NDGMV		56 (52–58)	57 (56–59)	0.10	49 (47–51)	53 (48–55)	**0.003**
N-Cortical volume		566 (330–566)	590 (475–750)	**0.019**	404 (332–498)	524 (399–633)	**0.023**
		Perivascular space enlargement					
		NMOSD (all, *n* = 34)			**HC (all, n = 46)**		***p***
Basal ganglia		2 (1–2)			1 (1–2)		0.17
n (%)[a]	Mild[b]	16 (47.1)			26 (56.5)		0.26
	Moderate[c]	13 (38.2)			18 (39.1)		
	Severe[d]	5 (14.7)			2 (4.3)		
Centrum semiovale		1 (1–3)			1 (0–2)		**0.034**
n (%)[a]	Mild[b]	19 (55.9)			29 (63.0)		**0.04**
	Moderate[c]	5 (14.7)			13 (28.3)		
	Severe[d]	10 (29.4)			4 (8.7)		

[a]*p* values refert to Fisher's exact test.
[b]PVS score: 0–1.
[c]PVS score = 2.
[d]PVS score = 3–4.
Data are presented as median (IQR), and *p* values refer to nonparametric Mann–Whitney *U* test, unless otherwise specified
HC = healthy controls; N- = normalized; NBV = normalized brain volume; NDGMV = normalized deep gray matter volume; NMOSD = neuromyelitis optica spectrum disorders; PVS = perivascular spaces; T2 LV = natural logarithm of T2 lesion volume.

space enlargement compared with HCs (29.4 vs 8.7%, $p = 0.040$). Details are provided in Table 2.

DTI-ALPS Index

The between-group comparison of aDTI-ALPS index is reported in Table 3.

1. Manual versus aDTI-ALPS index (exploratory dataset). Manual DTI-ALPS and aDTI-ALPS index showed an ICC of 0.97 (95% confidence interval 0.94–0.99, $p < 0.0001$, linear $R^2 = 0.91$; Figure, panel B).
2. Between-group comparisons of aDTI-ALPS index (exploratory dataset). NMOSD patients had a significant reduction of the aDTI-ALPS index compared with HCs ($p = 0.004$), whereas no differences were detected for FA and MD values (p values range 0.22–0.61).
3. Between-group comparisons of aDTI-ALPS index (validation-dataset). Compared with HCs, NMOSD patients showed a significant reduction of aDTI-ALPS ($p = 0.038$), with similar FA and MD values (p values range: 0.47–0.94).

Between-group comparison of aDTI-ALPS index (pooled analysis).The pooled analysis confirmed the reduction of aDTI-ALPS in NMOSD patients ($p < 0.001$; Figure, panel C).

Analysis of Correlations

In NMOSD patients, lower aDTI-ALPS correlated with higher EDSS (r −0.46, $p = 0.009$) and higher MD

TABLE 3. Between-Group Comparison of aDTI-ALPS Index

	Exploratory-dataset			Validation-dataset		
	NMOSD (n = 14)	HC (n = 16)	*p*	NMOSD (n = 20)	HC (n = 30)	*p*
aDTI-ALPS index	1.59 (1.53–1.69)	1.79 (1.66–1.90)	**0.004**	1.57 (1.48–1.64)	1.63 (1.54–1.79)	**0.038**
Mean FA_{ROI}	0.49 (0.48–0.52)	0.51 (0.65–0.68)	0.61	0.50 (0.48–0.53)	0.50 (0.49–0.52)	0.94
Mean MD_{ROI}[b]	0.68 (0.66–0.69)	0.66 (0.65–0.68)	0.22	0.70 (0.69–0.72)	0.71 (0.70–0.73)	0.47
	Pooled analysis[a]					
	NMOSD (all, n = 34)			**HC (all, n = 46)**		*p*
aDTI-ALPS index	1.58 (1.53–1.63)			1.71 (1.67–1.76)		**<0.001**
Mean FA_{ROI}	0.50 (0.49–0.51)			0.51 (0.50–0.51)		0.45
Mean MD_{ROI}[b]	0.70 (0.69–0.71)			0.70 (0.69–0.70)		0.64

[a]Age-, sex-, and scanner-adjusted general linear models; estimated mean (95% confidence interval).
[b]MD values are multiplied by 1,000.
Data are presented as median (IQR), and *p* values refer to nonparametric Mann–Whitney *U* test, unless otherwise specified
aDTI-ALPS = automated diffusion along perivascular spaces index; FA_{ROI} = mean fractional anisotropy within the two regions of interest (ROI_{proj} and ROI_{assoc}); HC = healthy controls; MD_{ROI} = mean mean diffusivity within the two regions of interest (ROI_{proj} and ROI_{assoc}); NMOSD = neuromyelitis optica spectrum disorders; ROI = region of interest.

within the ROIs ($r = -0.48$, $p = 0.006$). No further significant correlations were observed between aDTI-ALPS index and the other clinical and MRI variables, including disease duration.

Perivascular space scores in the basal ganglia and centrum semiovale were highly correlated ($r = 0.70$, $p < 0.0001$). Higher perivascular space score in the basal ganglia correlated with lower NDGM volume ($r = -0.44$, $p = 0.013$), whereas higher perivascular space score in the centrum semiovale correlated with lower normalized volumes of the brain ($r = -0.38$, $p = 0.036$), NDGM volume ($r = -0.36$, $p = 0.046$), and z-scores of the Paced Auditory Serial Addition Test 3″ ($r = -0.42$, $p = 0.03$).

No correlations were found between aDTI-ALPS index and perivascular space scores.

TABLE 4. Regression Models

Dependent variable	Significant IVs	Beta	Wald χ^2	*p*	Nagelkerke R^2
NMOSD Diagnosis	aDTI-ALPS index	−10.16	9.75	0.002	0.62
	NDGMV	$-3.78*10^{-3}$	10.04	<0.001	
	N-cortical volume	$-1.35*10^{-11}$	12.18	<0.001	
Dependent variable	**Significant IVs**	**Standardized beta**		*p*	**Adjusted R^2**
EDSS	No. myelitis	0.47		0.003	0.55
	aDTI-ALPS index	−0.33		0.033	
	logT2LV	0.38		0.035	

p values refer to age-, sex-, and scanner-adjusted binomial logistic regression (neuromyelitis optica spectrum disorders [NMOSD] diagnosis) or linear regression models (Expanded Disability Status Scale [EDSS]).
Only statistically significant independent variables are reported.
aDTI-ALPS = automated diffusion along perivascular spaces index; logT2LV = natural logarithm of T2 lesion volume; IVs = independent variables; NDGMV = normalized deep grey matter volume; N-cortical = normalized cortical.

Regression models

The results of age-, sex-, and scanner-adjusted logistic and linear regression models are shown in Table 4.

Independent predictors of NMOSD diagnosis were lower aDTI-ALPS index, NDGM volume, and normalized cortical volume (adjusted $R^2 = 0.62$).

Higher EDSS was associated with a higher number of myelitis, lower aDTI-ALPS index, and higher T2 lesion volumes (adjusted $R^2 = 0.55$).

No independent predictors of impairment in the information processing speed/attention domain were detected.

Discussion

In this work, we evaluated perivascular space abnormalities in patients with NMOSD, as disease pathogenesis involves the AQP4 water channel (ie, located in the perivascular space) and leads to damage of the astrocytes (ie, perivascular space boundaries).

For this purpose, we rated perivascular space enlargement with a well-established semiquantitative score (the Potter's score, the higher, the worse),[21] and measured water diffusion along perivascular spaces with the DTI-ALPS index in two independent cohorts of NMOSD patients and HCs.

Perivascular space enlargement in the centrum semiovale was more severe in NMOSD: approximately 30% of patients compared with <10% of age- and sex-matched HCs showed >20 MRI-visible Virchow–Robin spaces. Although many conditions have been associated with perivascular space enlargement in the basal ganglia (ie, aging, cardiovascular risk factors, and dementia),[30] perivascular space enlargement in the centrum semiovale is less associated with aging and is rarely seen in neurodegenerative or cerebrovascular disorders.

In contrast, prior investigations found an association between perivascular space enlargement in the centrum semiovale and inflammatory diseases, such as systemic lupus erythematosus,[31] multiple sclerosis,[32] and four aggressive cases of pediatric neuromyelitis optica,[33] suggesting that perivascular spaces might represent a route to central nervous system infiltration and circulation by leukocytes, therefore increasing in size during inflammation.[1]

When we considered microstructural water movement along perivascular spaces, we found a reduced aDTI-ALPS index in both datasets of NMOSD patients.

To note, as participants in the validation dataset were acquired almost 10 years before those in the exploratory dataset, we first compensated for the lack of the SWI sequence in the first group by setting up an automated system of ROI positioning based on the manual ROI probability map in the exploratory dataset. The obtained aDTI-ALPS index showed an almost perfect correspondence with the manual DTI-ALPS index (ICC = 0.97), thus allowing its use in the validation dataset.

Then, we took advantage of having two separate datasets to carry out two independent analyses of the aDTI-ALP index (ie, exploratory analysis and validation analysis), which was consistently reduced in NMOSD patients compared with HCs.

When we explored the clinical correlates, lower aDTI-ALPS index, together with deep GM and cortical atrophy, were independently associated with NMOSD diagnosis, in line with prior studies showing GM atrophy,[34,35] and a peculiar pattern of cortical AQP4 neuronal loss and nonlytic reaction of AQP4-negative astrocytes in NMOSD.[36]

However, no correlations between aDTI-ALPS index and Potter's score or MRI measures were found. In contrast, higher perivascular space enlargement correlated with brain and deep GM atrophy.

Beyond the technical limitations of the aDTI-ALPS index, changes in microstructural diffusivity might be more sensitive to early perivascular space abnormalities associated with NMOSD, whereas macroscopic evidence of perivascular space enlargement could suggest an overt process associated with subsequent mechanisms of neurodegeneration, as also supported by the correlation between higher Potter's score and poorer cognitive performance at Paced Auditory Serial Addition Test 3″.

Recent lines of research indicate that perivascular spaces might be involved in fluid and waste drainage as a part of a clearance system called "glymphatic". According to this hypothesis, brain clearance is promoted by the convective influx of the cerebrospinal fluid, which enters in the brain parenchyma along the periarteriolar space, reaches the interstitium through an astrocyte-dependent process, and is finally collected back in the perivenous space to drain out in the meningeal lymphatic vessels.[30,37] In this system, the AQP4 water channel is believed the leading promoter of cerebrospinal fluid flux through the glymphatic pathway,[38] as suggested by the 65% reduction of cerebrospinal fluid flow through the parenchyma in experimental models lacking AQP4.[30]

As the DTI-ALPS index was proposed as a noninvasive proxy for glymphatic functioning,[8] and considering the central role of AQP4, it is tempting to speculate that the perivascular space abnormalities detected in NMOSD might be due to impaired glymphatic functioning.

Indeed, a reduced DTI-ALPS index was detected in different neurological disorders, such as Alzheimer's disease,[8] Parkinson's disease,[10] idiopathic normal pressure hydrocephalus,[39] and, more recently, multiple sclerosis.[11]

The accumulation of protein aggregates and a reduced density of AQP4 water channels have been proposed as mechanisms of "glymphatic impairment" in neurodegenerative conditions, as the former would prevent

the normal perivascular outflow, whereas the latter would impair fluid drainage in the interstitium.[40]

So far, reduced glymphatic functioning in neuroinflammatory conditions was detected only in multiple sclerosis using the DTI-ALPS index or positron emission tomography imaging.[11,41] In this disease, both ongoing inflammation and neurodegeneration might contribute to this finding, as reduced glymphatic functioning correlated with white[11,41] and GM lesion volume,[11] but also greater abnormalities were observed in patients with progressive disease course, and worse cortical and deep GM atrophy.[11]

Similarly to NMOSD, loss of astrocyte endfeet[42] and astrocyte–oligodendrocyte connexins[43] have been observed in acute demyelinating lesions in multiple sclerosis. However, in contrast with NMOSD, where AQP4 immunoreactivity is lost at any stage of demyelination, AQP4 loss in multiple sclerosis is observed in inactive lesions, while its expression is increased at the border of active lesions, and in remyelinating lesions.[5]

In multiple sclerosis, DTI-ALPS index reduction correlated with EDSS, disease duration, and measures of brain atrophy.[11] This was partially in contrast with the present findings in NMOSD, where this index was associated with clinical disability, but unrelated to disease duration or brain atrophy.

This evidence might support an early impairment of glymphatic functioning in NMOSD, possibly associated with the disease pathophysiology. In fact, the magnitude of the pathogenic mechanism is likely to influence the severity of clinical manifestations, regardless of disease duration.

In contrast, the reduction of glymphatic functioning in multiple sclerosis could be secondary to inflammatory damage (ie, leukocyte infiltrates and astrocyte damage in active demyelinating lesions), and might fuel a vicious circle by prolonging the contact between brain tissue and detrimental factors (ie, cerebrospinal fluid, inflammatory cytokines, and reactive oxygen species), therefore triggering subsequent parenchymal damage and neurodegeneration.

However, the existence and functioning of the glymphatic system is still controversial, and its possible biological correlate deserves to be further investigated.

In NMOSD, another possibility is that the damage at the perivascular site, together with hyalinization around vessels[5] and gap junction enlargement,[44] might be responsible for the reduction of the DTI-ALPS index by altering perivascular space anatomy. Although we cannot exclude this possibility, we believe that this effect should be at least tempered on our data, as this index was not measured at small-caliber vessels level (ie, the capillary bed) and the visual check of aROI positioning avoided its measurement in correspondence of visible vascular or inflammatory focal abnormalities.

Moving to limitations, the rarity of the disease and the need of advanced sequences limited our sample size. However, the concordant results obtained in two different datasets encourage the future application of this method in a multicentric setting.

Second, the present study had a cross-sectional design; if perivascular abnormalities are secondary to the antibody-dependent pathogenetic mechanism of the disease, a longitudinal setting would better underpin changes associated with disease activity.

Third, there were intrinsic limitations of the technique itself. As the DTI-ALPS index is based on only two, small-sized ROIs in the left hemispheric WM, we cannot exclude the existence of a sampling bias.

Finally, in patients with NMOSD, concomitant vascular or autoimmune comorbidities, including connective tissue disorders and antiphospholipid syndrome might further contribute to the perivascular damage through an AQP4- and astrocyte-independent mechanism.

However, to the best of our knowledge, this is the first work systematically evaluating macroscopic and microstructural perivascular space abnormalities in NMOSD. By showing an association between reduced water diffusion along the perivascular spaces and both the presence of the disease and the severity of clinical disability, it also suggests a potential role of aDTI-ALPS index in the identification of NMOSD patients and in their monitoring. Future studies are warranted to better clarify the pathophysiological correlates of this finding and its clinical value.

Acknowledgment

Antonio Carotenuto is supported by a MAGNIMS/ECTRIMS research fellowship program. The work did not receive any additional funding.

Author Contributions

L.C., A.C., M.F., and M.A.R. contributed to the conception and design of the study. L.C., A.C., E.P., D.M., M.R., V.M., M.F., and M.A.R. contributed to the acquisition and analysis of data. L.C., A.C., E.P., D.M., M.R., V.M., M.F., and M.A.R. contributed to drafting the text and preparing the figures.

Potential Conflicts of Interest

Nothing to report.

References

1. Wuerfel J, Haertle M, Waiczies H, et al. Perivascular spaces--MRI marker of inflammatory activity in the brain. Brain 2008;131:2332–2340.

2. Wingerchuk DM, Banwell B, Bennett JL, et al. International consensus diagnostic criteria for neuromyelitis optica spectrum disorders. Neurology 2015;85:177–189.

3. Lucchinetti CF, Guo Y, Popescu BF, et al. The pathology of an autoimmune astrocytopathy: lessons learned from neuromyelitis optica. Brain Pathol 2014;24:83–97.
4. Saadoun S, Papadopoulos MC. Aquaporin-4 in brain and spinal cord oedema. Neuroscience 2010;168:1036–1046.
5. Roemer SF, Parisi JE, Lennon VA, et al. Pattern-specific loss of aquaporin-4 immunoreactivity distinguishes neuromyelitis optica from multiple sclerosis. Brain 2007;130:1194–1205.
6. Wardlaw JM, Benveniste H, Nedergaard M, et al. Perivascular spaces in the brain: anatomy, physiology and pathology. Nat Rev Neurol 2020;16:137–153.
7. Sepehrband F, Cabeen RP, Choupan J, et al. Perivascular space fluid contributes to diffusion tensor imaging changes in white matter. Neuroimage 2019;197:243–254.
8. Taoka T, Masutani Y, Kawai H, et al. Evaluation of glymphatic system activity with the diffusion MR technique: diffusion tensor image analysis along the perivascular space (DTI-ALPS) in Alzheimer's disease cases. Jpn J Radiol 2017;35:172–178.
9. Gouveia-Freitas K, Bastos-Leite AJ. Perivascular spaces and brain waste clearance systems: relevance for neurodegenerative and cerebrovascular pathology. Neuroradiology 2021;63:1581–1597.
10. Chen HL, Chen PC, Lu CH, et al. Associations among cognitive functions, plasma DNA, and diffusion tensor image along the perivascular space (DTI-ALPS) in patients with Parkinson's disease. Oxid Med Cell Longev 2021;2021:4034509.
11. Carotenuto A, Cacciaguerra L, Pagani E, et al. Glymphatic system impairment in multiple sclerosis: relation with brain damage and disability. Brain 2021. doi:10.1093/brain/awab454
12. Kurtzke JF. Rating neurologic impairment in multiple sclerosis: an expanded disability status scale (EDSS). Neurology 1983;33:1444–1452.
13. Cacciaguerra L, Valsasina P, Meani A, et al. Volume of hippocampal subfields and cognitive deficits in neuromyelitis optica spectrum disorders. Eur J Neurol 2021;28:4167–4177.
14. Meng H, Xu J, Pan C, et al. Cognitive dysfunction in adult patients with neuromyelitis optica: a systematic review and meta-analysis. J Neurol 2017;264:1549–1558.
15. Amato MP, Portaccio E, Goretti B, et al. The Rao's brief repeatable battery and Stroop test: normative values with age, education and gender corrections in an Italian population. Mult Scler 2006;12:787–793.
16. Sumowski JF, Benedict R, Enzinger C, et al. Cognition in multiple sclerosis: state of the field and priorities for the future. Neurology 2018;90:278–288.
17. Valverde S, Cabezas M, Roura E, et al. Improving automated multiple sclerosis lesion segmentation with a cascaded 3D convolutional neural network approach. Neuroimage 2017;155:159–168.
18. Battaglini M, Jenkinson M, De Stefano N. Evaluating and reducing the impact of white matter lesions on brain volume measurements. Hum Brain Mapp 2012;33:2062–2071.
19. Smith SM, Zhang Y, Jenkinson M, et al. Accurate, robust, and automated longitudinal and cross-sectional brain change analysis. Neuroimage 2002;17:479–489.
20. Patenaude B, Smith SM, Kennedy DN, Jenkinson M. A Bayesian model of shape and appearance for subcortical brain segmentation. Neuroimage 2011;56:907–922.
21. Potter GM, Chappell FM, Morris Z, Wardlaw JM. Cerebral perivascular spaces visible on magnetic resonance imaging: development of a qualitative rating scale and its observer reliability. Cerebrovasc Dis 2015;39:224–231.
22. Andersson JLR, Graham MS, Drobnjak I, et al. Towards a comprehensive framework for movement and distortion correction of diffusion MR images: within volume movement. Neuroimage 2017;152:450–466.
23. Basser PJ, Mattiello J, LeBihan D. MR diffusion tensor spectroscopy and imaging. Biophys J 1994;66:259–267.
24. Abdul-Rahman HS, Gdeisat MA, Burton DR, et al. Fast and robust three-dimensional best path phase unwrapping algorithm. Appl Optics 2007;46:6623–6635.
25. Sun H, Wilman AH. Background field removal using spherical mean value filtering and Tikhonov regularization. Magn Reson Med 2014;71:1151–1157.
26. Alexander DC, Pierpaoli C, Basser PJ, Gee JC. Spatial transformations of diffusion tensor magnetic resonance images. IEEE Trans Med Imaging 2001;20:1131–1139.
27. Taoka T, Ito R, Nakamichi R, et al. Reproducibility of diffusion tensor image analysis along the perivascular space (DTI-ALPS) for evaluating interstitial fluid diffusivity and glymphatic function: CHanges in Alps index on multiple conditiON acquIsition eXperiment (CHAMONIX) study. Jpn J Radiol 2022;40:147–158.
28. Ringstad G, Vatnehol SAS, Eide PK. Glymphatic MRI in idiopathic normal pressure hydrocephalus. Brain 2017;140:2691–2705.
29. Smith SM, Jenkinson M, Johansen-Berg H, et al. Tract-based spatial statistics: voxelwise analysis of multi-subject diffusion data. Neuroimage 2006;31:1487–1505.
30. Jessen NA, Munk AS, Lundgaard I, Nedergaard M. The Glymphatic system: a Beginner's guide. Neurochem Res 2015;40:2583–2599.
31. Wiseman SJ, Bastin ME, Jardine CL, et al. Cerebral small vessel disease burden is increased in systemic lupus erythematosus. Stroke 2016;47:2722–2728.
32. Troili F, Cipollini V, Moci M, et al. Perivascular unit: this must be the place. The anatomical crossroad between the immune, vascular and nervous system. Front Neuroanat 2020;14:17.
33. Zhang Z, Zhou H, Liu X, et al. Identification of the clinical and neuroimaging characteristics in children with neuromyelitis optica spectrum disorders: a case series. Transl Pediatr 2021;10:2459–2466.
34. Hyun JW, Park G, Kwak K, et al. Deep gray matter atrophy in neuromyelitis optica spectrum disorder and multiple sclerosis. Eur J Neurol 2017;24:437–445.
35. Tian DC, Xiu Y, Wang X, et al. Cortical thinning and ventricle enlargement in Neuromyelitis Optica Spectrum disorders. Front Neurol 2020;11:872.
36. Saji E, Arakawa M, Yanagawa K, et al. Cognitive impairment and cortical degeneration in neuromyelitis optica. Ann Neurol 2013;73:65–76.
37. Iliff JJ, Wang M, Liao Y, et al. A paravascular pathway facilitates CSF flow through the brain parenchyma and the clearance of interstitial solutes, including amyloid beta. Sci Transl Med 2012;4:147ra111.
38. Iliff JJ, Nedergaard M. Is there a cerebral lymphatic system? Stroke 2013;44:S93–S95.
39. Yokota H, Vijayasarathi A, Cekic M, et al. Diagnostic performance of Glymphatic system evaluation using diffusion tensor imaging in idiopathic Normal pressure hydrocephalus and mimickers. Curr Gerontol Geriatr Res 2019;2019:5675014.
40. Hasan-Olive MM, Enger R, Hansson HA, et al. Loss of perivascular aquaporin-4 in idiopathic normal pressure hydrocephalus. Glia 2019;67:91–100.
41. Schubert JJ, Veronese M, Marchitelli L, et al. Dynamic (11)C-PiB PET shows cerebrospinal fluid flow alterations in Alzheimer disease and multiple sclerosis. J Nucl Med 2019;60:1452–1460.
42. Prineas JW, Lee S. Multiple sclerosis: destruction and regeneration of astrocytes in acute lesions. J Neuropathol Exp Neurol 2019;78:140–156.
43. Masaki K, Suzuki SO, Matsushita T, et al. Connexin 43 astrocytopathy linked to rapidly progressive multiple sclerosis and neuromyelitis optica. PLoS One 2013;8:e72919.
44. Richard C, Ruiz A, Cavagna S, et al. Connexins in neuromyelitis optica: a link between astrocytopathy and demyelination. Brain 2020;143:2721–2732.